RESEARCH ARTICLE

[M]acro-
[M]olecular
Materials and Engineering
Open Access

www.mame-journal.de

Biomimetic Polycaprolactone-Graphene Oxide Composites for 3D Printing Bone Scaffolds

Iman Sahafnejad-Mohammadi, Sadegh Rahmati, Najmeh Najmoddin, and Mahdi Bodaghi*

Bone shows a radial gradient architecture with the exterior densified cortical bone and the interior porous cancellous bone. However, previous studies presented uniform designs for bone scaffolds that do not mimic natural bone's gradient structure. Hence, mimicking native bone structures is still challenging in bone tissue engineering. In this study, a novel biomimetic bone scaffold with Haversian channels is designed, which approximates mimicking the native bone structure. Also, the influence of adding graphene oxide (GO) to polycaprolactone (PCL)-based scaffolds are investigated by preparing PCL/GO composite ink containing 0.25% and 0.75% GO and then 3D printing scaffolds by an extrusion-based machine. Scanning electron microscopy (SEM) is used for morphological analysis. SEM reveals good printability and interconnected pore structure. The contact angle test shows that wettability reinforces with the increase of GO content. The mechanical behavior of the scaffolds under compression is examined numerically and experimentally. The results indicate that incorporation of GO can affect bone scaffolds' Young's modulus and von Mises stress distribution. Moreover, the biodegradation rates accelerate in the PCL/GO scaffolds. Biological characterizations, such as cell growth, viability, and attachment, are performed utilizing osteoblast cells. Compared to pure PCL, an enhancement is observed in cell viability in the PCL/GO scaffolds.

1. Introduction

Annually, millions of patients suffer from significant bone defects due to trauma, accident, cancer, infection, or faulty developmental processes.[1] To date, the main guideline for these defects is auto-grafts, allografts, and xenografting which suffer from some drawbacks such as limited bone donor supply, indicating insufficient reproducibility, limited ability to adjust pore geometry and pore size, the necessity of additional surgery and immune rejection.[2–4] Hence, to address these issues, bone tissue engineering has been introduced to regenerate specific and functional human bone tissue.[5] Scaffolds play a central role in tissue engineering and serve as a temporary template to provide structural supports for guiding cells and constructing new tissue.[6,7] Ideally, the scaffold for such applications has to fulfill the following requirements, i) a 3D, porous structure with desirable surface chemistry to support cell growth, proliferation, and differentiation,[8,9] ii) open and interconnected pores for mass transport,[10] iii) a biocompatible and biodegradable substrate with tuned degradation rate with tissue ingrowth,[11] and iv) having mechanical features similar to the tissues at the site of implantation.[8]

Polycaprolactone (PCL) is a synthetic, biocompatible, biodegradable, non-toxic, and simply obtainable aliphatic polyester that a U.S. Food and Drug Administration (FDA) certified as a safe biomaterial.[12,13] However, PCL has a minimal bioactivity and cell adhesion due to its non-osteogenic nature and inherent hydrophobic surface. Incorporation of inorganic substances to the PCL scaffold is a common strategy to improve its hydrophilicity.[14] Among various additives, graphene oxide (GO) as an excellent 2D material has been fascinated to bring attention toward its superb properties such as excellent flexibility, high Young's modulus and also hydrophilic oxygen-containing groups such as epoxy, carboxyl, and hydroxyl on its surface.[6,15] Song et al. reported that incorporation of GO nano-sheets dramatically enhanced the differentiation of mouse marrow mesenchymal stem cells (mMSCs) into osteo-like cells, which further proved the excellent biocompatibility of GO.[6] Unagolla et al. stated that PCL scaffold containing 0.5% GO was the most favorable for cell proliferation and differentiation.[16] Zhang et al. revealed that 3D bio-printed cell-laden scaffolds with 1 mg ml^{-1} GO incorporation improved osteogenic differentiation and mineralization.[17] Moreover, many researchers showed the

I. Sahafnejad-Mohammadi, S. Rahmati, N. Najmoddin
Department of Biomedical Engineering, Science and Research Branch
Islamic Azad University
Tehran Iran
M. Bodaghi
Department of Engineering, School of Science and Technology
Nottingham Trent University
Nottingham NG11 8NS, UK
E-mail: mahdi.bodaghi@ntu.ac.uk

The ORCID identification number(s) for the author(s) of this article can be found under https://doi.org/10.1002/mame.202200558

ADVANCED SCIENCE NEWS
www.advancedsciencenews.com

Macro-molecular Materials and Engineering
Open Access
www.mame-journal.de

Figure 1. Design of biomimetic bone scaffold: a) native bone structure, b) CAD design of the biomimetic bone scaffold.

positive role of graphite derivatives on the bioactivity, biocompatibility, and biodegradability of PCL-based scaffolds.[18,19] For instance, Wang et.al fabricated PCL/graphene (G) composites scaffolds and characterized them.[20] The study demonstrated that the PCL/G scaffolds cause an appropriate level of an immune response, indicating a high potential for in vivo applications.[20]

It is essential to evaluate the mechanical properties of a bone tissue engineering scaffold in detail.[21] The stress shielding phenomenon occurs in case of higher strength of scaffold than that of the surrounding bone. On the other hand, the scaffold will probably fail before cell growth, if the scaffold is weaker than the surrounding environment.[22] Mechanical properties of scaffolds can be tuned by the scaffold material as well as scaffold microstructure. So, it is crucial to develop a construct which collectively recapitulate gradients found in native osteochondral tissues. On the micro-scale, the natural bone has a functionally graded structure with a diverse pore size and porosity distribution.[23] For instance, the outer compact bone layer has a porosity between 5% and 30% (often in the range of 5%–10%), while the internal spongy bone indicates a trabecular structure, which varies from 50% to 90%.[23,24] In other words, native bone is composed of cortical bone (containing Haversian channels) at the exterior layer and cancellous bone (containing trabecular beams) at the interior, see **Figure 1**a. Cortical bone is extremely densified and supplies the major mechanical strength of bone; however, the main bone healing processes happen in cancellous bone.[25] Most of the produced scaffolds have a uniform design which does not satisfy the radial-gradient of porosity in different regions of the natural bone.[23,25] Consequently, the production of bone scaffolds with biomimetic design containing cortical and cancellous regions with predefined porosity is still challenging in bone tissue engineering.

Additive manufacturing or 3D printing is a cutting-edge technology that allows the product of complicated geometries with excellent resolution and high precision control.[26] Also, 3D printing is a potential approach for creating bone scaffolds with regulated physical and mechanical characteristics with hierarchical design.[27] This technology addresses the constraints of traditional scaffold manufacturing methods. Among the variety

of 3D printing methods available, cost-effective extrusion-based 3D printing has shown considerable potential in improving the creation of functional tissue replacement.[28,29] By utilizing the computer-aided design (CAD), pore geometry and size, strand size, and material composition could be designed before printing. The finite element (FE) method as a computational technique for modeling and simulation of various domains is a strong tool to design and analysis of 3D tissue structures.[30,31,21] Owing to the capability of the CAD-based FE approach to supply high precision in optimizing the geometric design, utilizing FE method's ability to predict the mechanical behaviors of the tissue-engineered scaffolds could be practical for tissue engineering applications.[32,33]

As mentioned above, native bones do not have a homogeneous structure, as they are composed of two parts, namely cortical and cancellous regions, that show the gradient structures of bone. However, most of the fabricated scaffolds have a uniform and simple design that does not satisfy the radial gradient of porosity in different regions of the natural bone. Consequently, the fabrication of bone scaffolds with biomimetic design and distinguishing in porosity between cortical and cancellous regions is still challenging in bone tissue engineering. Therefore, in this present study, inspired by gradient structures of native bone, biomimicking bone scaffolds containing cortical (along with Haversian canals) and cancellous regions with a different number of strands are successfully manufactured through an extrusion-based 3D printing technology. In this regard, the scaffold is first designed, and 3D printed according to Figure 1b. It has been reported that 4 Haversian channels with a diameter in the range of 800—1600 μm are normally appropriate for mechanical performance, angiogenesis, and neurogenesis.[25] Then, the effects of GO content (0%, 0.25%, and 0.75%) and the number of strands in a cancellous section of scaffold (4 × 4 and 5 × 5) on the morphological properties, printability, crystallinity, and wettability of the scaffold are evaluated. Also, the mechanical behavior of the 3D printed scaffolds under uniaxial compression load is studied using experimental test and FE modeling. Furthermore, in vitro assessments, including biodegradability, swelling rate, MTT assay, and cell attachment, are performed in the presence of MG-63 osteoblast cells line to investigate the 3D printed scaffolds'

**ADVANCED
SCIENCE NEWS**

www.advancedsciencenews.com

[M]acro-
molecular
Materials and **Engineering**
Open Access

www.mame-journal.de

capability to regenerate tissue based on bone tissue engineering guidelines.

2. Experimental Section

2.1. Materials

Poly (ϵ-caprolactone) (PCL) (M_w: 80,000 g mol^{-1}) granules were supplied by Sigma-Aldrich (USA). The GO powders were purchased from Fine-Nano Co., LTD. Chloroform solvent was purchased from Co. Merck (Germany). All materials were used as received.

2.2. Preparation of PCL/GO Nanocomposite Inks

4 g of PCL granules were added to 20 ml of chloroform and completely dissolved under the stirring at 500 rpm for 4 h (**Figure 2**a, step i). 0.25% (w/w) and 0.75% (w/w) of GO concentrations were obtained by mixing 10 and 30 mg of GO powders, respectively, into the PCL solution under continuous stirring at 500 rpm for 24 h at room temperature (RT) to achieve a homogenous suspension (Figure 2a, step ii). To ensure the fully dispersion of GO in the PCL solution, the suspension was sonicated for another 1 h (Figure 2a, step iii). Then, the mixture was poured into a petri dish and left at RT overnight to evaporate the solvent (Figure 2a, step iv). Next, solid sheets were crushed to be ready for loading into the 3D bioprinter's syringe cartridge. The schematic representation of ink preparation depicted in Figure 2a.

2.3. Design and 3D Printing of Bio-Mimetic Scaffolds

In order to replicate the natural structure of a bone, a 3D digital model of scaffold with the cylindrical shape (2 mm thickness × 15 mm diameter) was designed with a distinct cortical and the cancellous regional using SolidWorks software package (Version 2016, Dassault Systems, France) (Figure 2b, step i). To investigate the effects of the pore size in the middle section of the scaffold (cancellous region), on the mechanical properties of the scaffolds, two different pore size, 700 μm (5 × 5 strands pattern) and 900 μm (4 × 4 strands pattern) were designed (Figure 2b, step ii and iii). Each layer of the scaffold in the cancellous region is square and has an interconnected lattice design with 0°/90° laydown patterns. The theoretical porosity of scaffolds was evaluated from the CAD data by volumes as follows (Equation 1):

$$P_{Throry} = \left(1 - \frac{V_{Theory}}{V_{Bulk}}\right) \times 100 \tag{1}$$

where V_{Theory} was the theoretical volume of porous scaffold and V_{Bulk} was the bulk volume of a non-porous cylinder with the same dimensions.

For all groups, cylindrical scaffolds with 25 layers were created as digital models, exported as STL format, and imported into Simplify3D (Cincinnati, OH, USA) software to generate device-readable G-code files. The fabrication of scaffolds conducted through BioFabX2 extrusion-based 3D bio-printer (Figure 2b, step ii). Briefly, the neat PCL and PCL/GO composite inks with 0.25% (w/w) and 0.75% (w/w) of GO concentrations were loaded to steel syringe and heated up to 90 °C and extruder pressure set up at 2 bar. Other parameters of printing processes were described in **Table 1**.

2.4. Characterization

The morphological analysis of PCL and PCL/GO composite scaffolds containing 0.25% (w/w) and 0.75% (w/w) of GO concentration was performed by scanning electron microscopy (SEM) (AIS 2100, Seron Technology, South Korea). The samples were sputter coated with a gold layer and then the images of scaffolds were captured at three magnifications at an accelerating voltage of 15 kV. The average diameter of Haversian channels and pore size was obtained from random measurements of the six pore regions on a typical SEM image through ImageJ software (1.52V, NIH, USA). The experimental porosity (P_{EXP}) of PCL and PCL/GO scaffold containing 0.25% (w/w) and 0.75% (w/w) of GO concentrations calculated from Equation (2).

$$P_{Exp} = \left(1 - \frac{M}{\rho V_{Bulk}}\right) \times 100 \tag{2}$$

in which M is the weight of the 3D printed scaffold, ρ is the PCL density (1.145 g cm^{-3}), and V_{Bulk} is the bulk volume of a nonporous cylinder with the same scaffold dimensions.

The crystalline structure of GO powders as well as scaffolds was carried out using an X-ray diffractometer (EQUINOX3000, Inel, France). The X-ray diffraction (XRD) was performed over a range of $2\theta = 0° - 70°$ with a voltage = 40 kV, current = 30 mA, step size of 0.01°, and time per step = 1 s. The crystalline phases and characteristic peaks were determined by X-Pert High-Score Plus software (Malvern Panalytical Ltd, Malvern, United Kingdom).

To study wettability of the scaffolds, water contact angle test was performed via contact angle analyzer (Data physics OCA15). 4 μL of deionized water were dropped onto scaffolds ($n = 4$). The water absorption of samples was recorded by a video contact angle system and the measurements were carried out by ImageJ software (1.52V, NIH, USA).[34]

The degradation study of the 3D printed scaffolds was examined by measuring the percentages of weight loss and swelling rate of research groups submerged in simulated body fluid (SBF) solution at pH 7.4, during 5, 10, and 15 days. To this end, the 3D printed scaffolds without or with 0.25% (w/w) and 0.75% (w/w) concentration of GO nanoparticles were accurately weighed and submerged in 15 mL of SBF and kept under gentle agitation at 37 °C for different time periods (0, 5, 10, and 15 days). Then the samples were removed, dried thoroughly, and weighed. The weight changes during the test were documented, and the weight loss for each scaffold as a degradation criterion was determined using the Equation (3):

$$Weight\ loss\ \% = \frac{W_0 - W_f}{W_0} \times 100 \tag{3}$$

where W_0 is the initial weight, and W_f is the degraded weight of the scaffold.
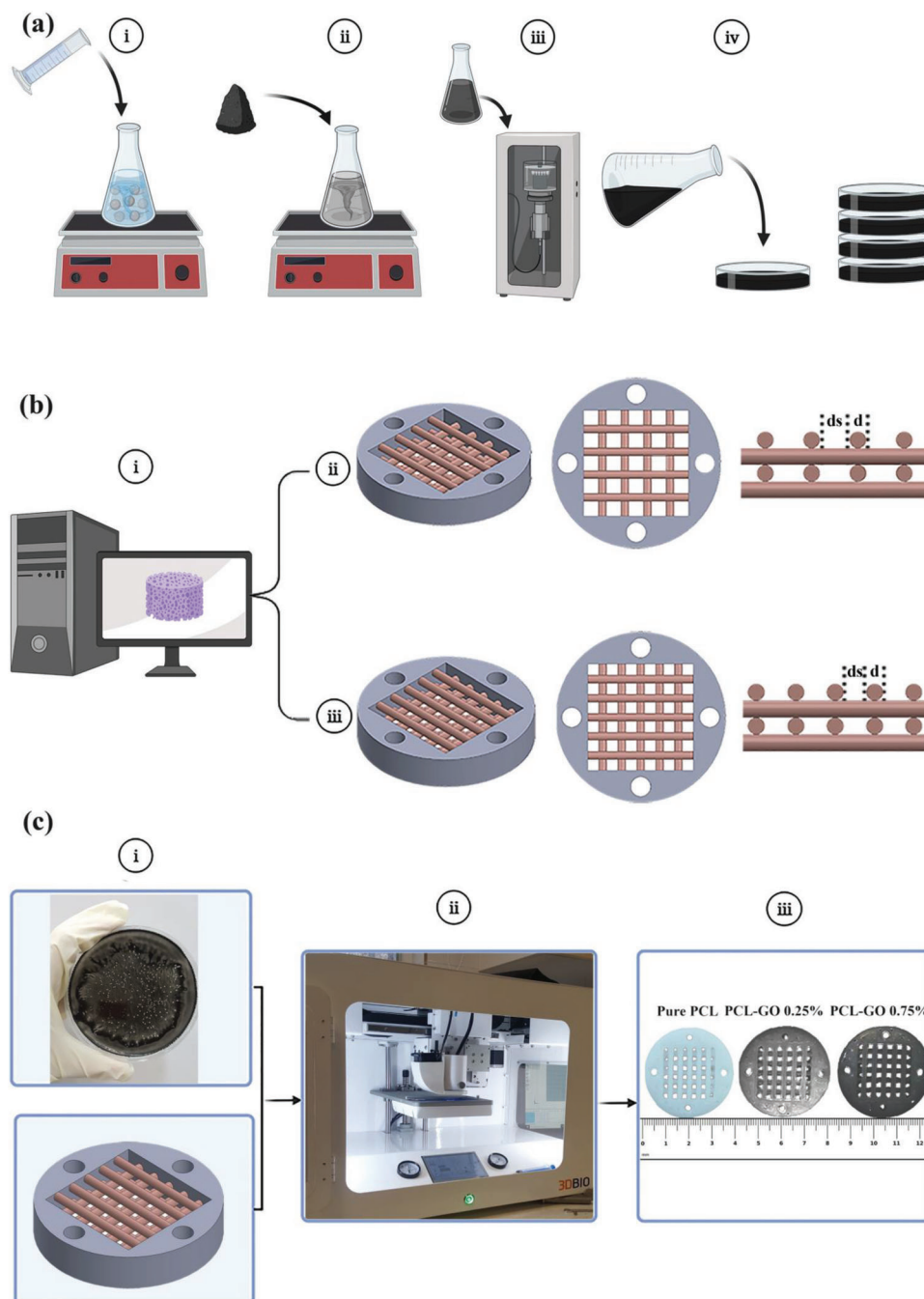
Figure 2. a) A schematic representation of the preparation of PCL/GO ink: i) PCL solution, ii) PCL/GO suspension, iii) ultrasonication of the mixture, iv) preparation of PCL/GO composite sheets. b) i) CAD models of the biomimetic bone scaffold designed by SolidWorks software, ii) 5 × 5 strand design (700 μm), iii) 4 × 4 strand design (900 μm). c) 3D printing and final products: i) integration of CAD models with ink, ii) 3D printing processes, iii) images of the final 3D printed scaffolds.

The SBF absorption experiment was carried out to assess the swelling rate of the 3D printed scaffolds. Briefly, the dry weight of samples was put into a container containing 15 ml of SBF (at natural pH) and incubated for 5, 10, and 15 days at 37 °C. Subsequently, the wet weight of the samples was measured by weighing them, instantly after removing the SBF solution from the surface of the 3D printed scaffolds with a fine filter paper.

Finally, the percentage rate of swelling was evaluated using the Equation (4):

$$Swelling\ rate = \frac{W_w - W_d}{W_d} \times 100 \tag{4}$$

where W_w is the wet weight, and W_d was the dry weight.

**ADVANCED
SCIENCE NEWS**

www.advancedsciencenews.com

acro-
olecular
Materials and Engineering
Open Access

www.mame-journal.de
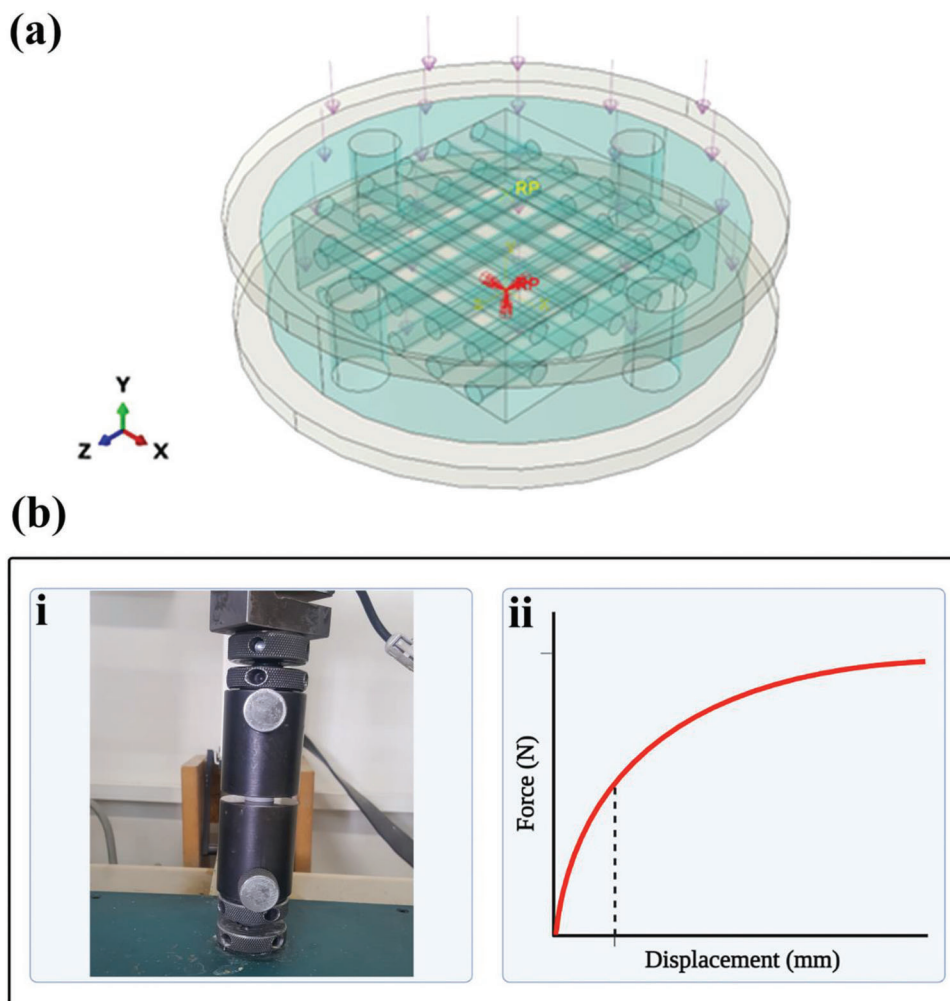
Figure 3. Methodology of mechanical investigations. a) creation for the finite element analysis. An instance of compressive forcing in the vertical direction is depicted. The bottom rigid plate is fixed (red RP), and the top rigid plate (yellow RP) moves downwards in the vertical axis. b) i) universal material testing machine, ii) a schematic diagram of Force-Displacement curve.

Table 1. Extrusion-based 3D printing parameters.

Parameters			
Nozzle diameter (mm)	0.5	Nozzle temp (°C)	90
Layer thickness (mm)	0.25	Print bead temp (°C)	30
Layer width (mm)	0.45	Print speed (mm/s)	2.5
Layer height (mm)	0.2	Extruder pressure (bar)	2

2.5. Finite Element Analysis

Finite element simulations were performed to study the influence of GO content on Young's modulus of 3D printed PCL-based scaffolds (0, 0.25% and 0.75% GO) under uniform 5% compression strain. Also, FE modelling was utilized to assess von Mises stress and its distribution in 3D printed scaffolds. Therefore, the commercial software (ABAQUS/Standard 6.14, Simulia, Dassault Systèmes, Farance) finite element tool was used to predict the mechanical characteristics of the biomimetic-designed tissue-engineered bone scaffolds under uniaxial compression load. To create FE models in the preprocessing step, the CAD data of each specimen was imported into the program as an ongoing part. The Young's modulus and Poisson's ratio of PCL has been reported to be 34.9 MPa and 0.3, respectively.[44] The scaffold models used in finite element modelling were discretized using linear tetrahedral elements. It is worth noting that one of the main aspects of FE analysis was the reliance of its result correctness on the mesh size; Hence the FE model with coarse mesh was not representational of the continuous model and leads to departure from precise findings.[45] Therefore, a mesh sensitivity test was conducted by consistently reducing the mesh size (or increasing the number of elements) to obtain mesh size-independent results. After doing this analysis, a proper mesh size for the FE models was achieved for the subsequent FE study.

The compression testing simulation was performed using the FE analysis of each model design. **Figure 3**a depicts the configuration of a simulation of the compression test in the vertical direction. Briefly, the scaffold specimen was placed between two rigid plates and the bottom of the model was fixed as boundary

ADVANCED
SCIENCE NEWS

www.advancedsciencenews.com

Macro-
molecular
Materials and Engineering
Open Access

www.mame-journal.de

conditions. Then, the 5% compressive strain was applied to the top of the scaffold to simulate the uniaxial compression test in the static condition. The displacement rate was 1 mm min^{-1}, which was a common quasi-static loading rate for bone and biomaterial analysis.[35] The compression load was determined for each model in the post-processing step. Thereafter, compressive Young' modulus (E) was examined from Equation (5):

$$E_{FEM} = \frac{F_{FEM}}{A \times \varepsilon_{FEM}} \tag{5}$$

in which, F_{FEM} is compression load at the end of the simulation processes, A is the initial area of cylindrical scaffold under compression force, and ε_{FEM} was a compressive strain of 5%.

2.6. Mechanical Investigation

In order to study the effect of GO content and pore size, on the mechanical behaviors of the 3D printed scaffolds, uniaxial compression tests were conducted as shown in Figure 3b. The 3D printed scaffolds were tested on a universal mechanical tester (H10KS, Hounsfield Co., UK) equipped with a 10 kN load cell (Figure 3b, step i). Each scaffold was compressed to a strain of around 30% at a rate of 1 mm min^{-1}. The experiments were conducted both in the air at room temperature and in phosphate buffered saline (PBS) (at neutral pH) at 37 °C for dry and wet conditions, respectively. The preparation of samples for wet mode measurements consisted of 1 h of immersion in PBS prior to the test. In the following, the scaffolds were then removed in PBS at 37 °C for 15 min to reach the testing temperature. The compressive Young's modulus was calculated from the linear elastic region of the compressive stress-strain curve (from 0 to 0.2% strain) and compressive strength values were evaluated according to the maximum compressive stress at 30% strain (Figure 3b, step ii). The experiments were run in triplicate.

2.7. In Vitro Biological Characterization

2.7.1. Cell Culture

Osteoblast cells (MG-63) were purchased from the Pasteur Institute of Iran's cell bank in order to investigate the in vitro cellular behavior of the 3D printed PCL-based scaffolds with different concentrations of GO nanoparticles. To this end, osteoblast cells were cultured in Dulbecco's modified Eagle medium (DMEM, Gibco) that was supplemented with 10% fetal bovine serum (FBS, Germany) and 100 U mL^{-1} penicillin (Sigma-Aldrich, USA). MG-63 cells were subsequently kept in a cell culture incubator at 37 °C, humidified, and exposed to 5% CO_2, and the culture environment was renewed every 3 days. Both sides of the samples were UV-sterilized for 45 min in advance. Samples were then transferred to 12-well plates. The 12-well plates were put, for 14 days in a cell culture incubator. The environment was renewed every 3 days over this period of time. On the 1st, 7th, and 14th days, samples were taken to evaluate the outcomes of the cell culture.

2.7.2. Cell Viability and MTT Assay

To study cell viability, the toxicity of the 3D-printed scaffolds was evaluated by MTT 3-(4,5-dimethylthiazol-2-yl)-2,5- diphenyltetrazolium bromide after the 1st, 7th and 14th days of the initial cell seeding. To achieve this, 500 μL of culture medium containing 10^4 cells mL^{-1} and 50 μL MTT solution were added to each sterile sample on a 12-well plate. The plates were incubated in an incubator for 4 h at 37 °C. After incubation in an incubator, the MTT labelling regent was aspirated, and then a solubilization buffer was added to dissolve the formazan crystals that formed. Finally, the absorbance values were determined at 540 nm using a microplate reader, and the viability of the cells was evaluated. The experiments run in triplicate.

2.7.3. Observation Cell Adhesion and Morphology with SEM

SEM images were taken on the 1st and 7th days of the MG-63 osteoblast cells culture in order to assess the adhesion and morphological properties of the cells on the cultured composite scaffolds. To this end, scaffolds were washed 3 times with PBS to remove nonattached osteoblast cells from the sample structure. Following that, the scaffolds were fixed by immersing in 2.5% glutaraldehyde in PBS at room temperature for 1 h. Subsequently, the specimens, were dehydrated for 15 min sequentially by several washing steps in graded ethanol (from 10% to 100% concentration). Finally, dehydration was finished by critical-point drying with CO_2. Scaffolds were sputtered coated with a thin layer of gold via a sputter coater under a high vacuum before being characterized with SEM.

2.8. Statistical Analysis

All experimental data were reported as mean ± standard deviation (SD). The statistical analysis was performed by one-way analysis of variance (one-way ANOVA) and two-way analysis of variance (two-way ANOVA) using GraphPad Prism software. Significant levels were determined at *$p < 0.05$, **$p < 0.01$, ***$p < 0.001$, and ****$p < 0.0001$.

3. Results and Discussion

To mimic the bone structure and rebuild the regeneration mechanism of damaged tissue, bio-mimetic bone scaffolds with cortical region along with Haversian channels, and the cancellous region along with interconnected lattice structure are designed and manufactured through an extrusion-based 3D bio-printer. Polycaprolactone (PCL) as a biopolymer is used due to its suitable biocompatibility and good printability with extrusion 3D printing technology. Despite the advantages of PCL, the inherent hydrophobicity of this material led us to add GO (0.25% (w/w) and 0.75% (w/w)) to address this issue and consequently enhance cell behavior. Finally, the six bio-mimetic bone scaffolds with different GO content and pore size in a cancellous section are successfully printed to investigate the effect of the mentioned variables on the morphological, physical, mechanical, and biological features of the samples. This section is dedicated to a discussion on the results.
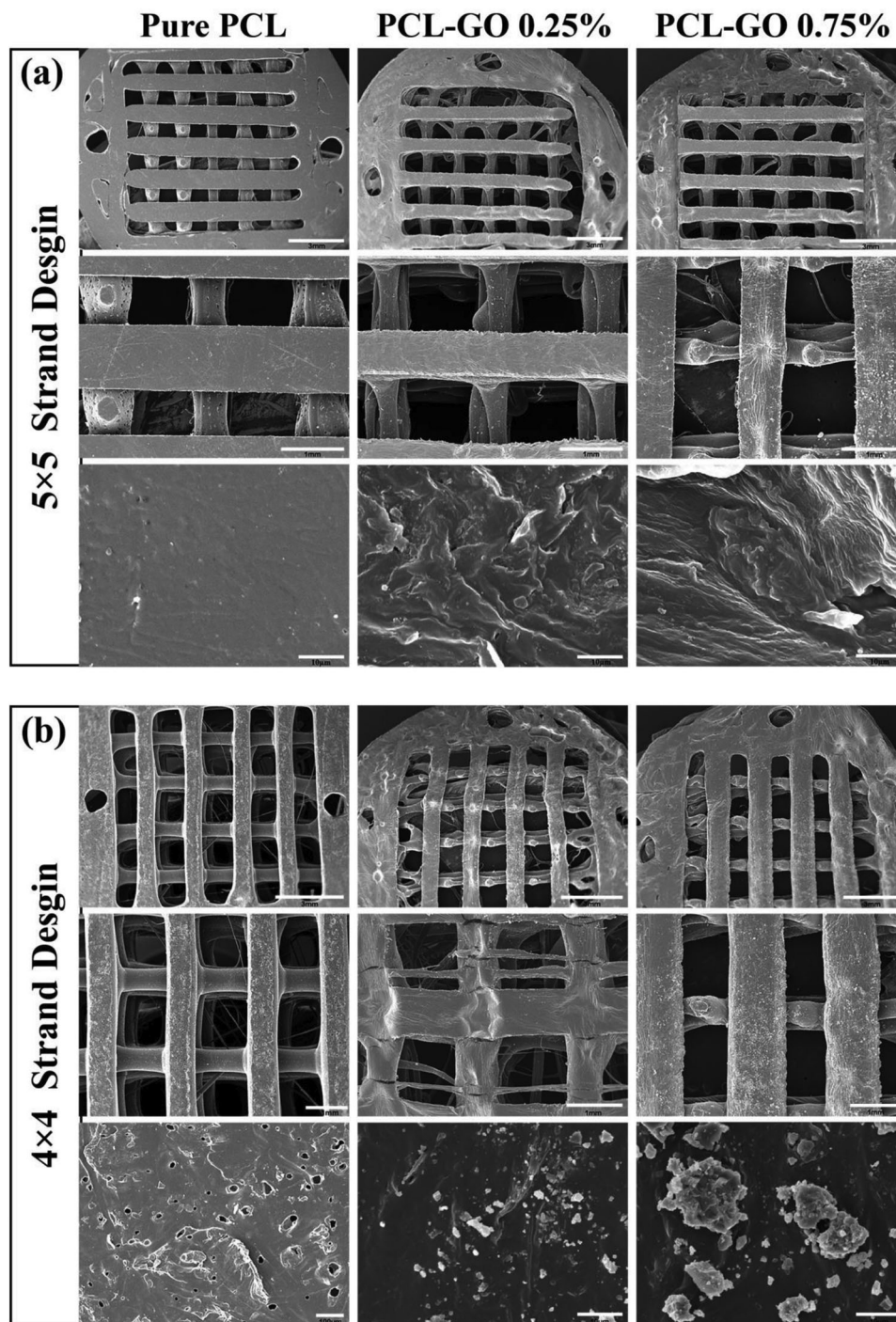
Figure 4. SEM images of biomimetic bone scaffolds made of different strands designs and GO content (0, 0.25% and 0.75%).

3.1. Morphological Features of 3D Printed PCL/GO Scaffolds

Figure 4 shows SEM images of the micro-structure of 3D printed scaffolds with different GO content and pore size, on a microscopic view. The scaffolds are 3D-printed with a regular structure and interconnected pores. The top-view of scaffolds indicates the regularity of the strands and the consistency of the 3D printing process across the different part of samples. It is evident that the

GO sheets protrude from the surface, generating a wrinkled topography, with surface roughness and irregularity which is more pronounce for 0.75% GO.

The desirable pore dimension and porosity of the scaffold can promote osteogenesis, neurogenesis, and angiogenesis, during bone healing processes.[36,37] In other words, average porosity sizes can seriously affect the preservation of the scaffolds' physicochemical and mechanical features; thus, it can effectively

ADVANCED
SCIENCE NEWS
www.advancedsciencenews.com

{M}acro-
molecular
Materials and Engineering
Open Access
www.mame-journal.de

Table 2. Comparison of CAD and experimental measurement of six types of scaffolds with different GO concentrations and pore size.

	CAD Haversian channel diameter [µm]	SEM Haversian channel diameter [µm]	CAD pore Size [µm]	SEM pore Size [µm]	Theoretical porosity [%]	Experimental porosity [%]
Pure PCL (5 × 5)	1200	1210 ± 20	700	721 ± 115	61.3	64.9
PCL/GO 0.25% (5 × 5)	1200	1184 ± 240	700	845 ± 173	61.3	66.7
PCL/GO 0.75% (5 × 5)	1200	1175 ± 130	700	895 ± 255	613	67.9
Pure PCL (4 × 4)	1200	1208 ± 33	900	955 ± 120	66.5	70.1
PCL/GO 0.25% (4 × 4)	1200	1240 ± 190	900	991 ± 170	66.5	72.6
PCL/GO 0.75% (4 × 4)	1200	1225 ± 120	900	998 ± 215	66.5	73.1

support the cellular behaviors.[38] Therefore, the average diameter of pore size, as well as the porosity of the 3D printed scaffolds, are measured and reported in **Table 2**. As can be seen, the pore size and porosity of the printed samples are higher than theoretical ones. Moreover, increasing the GO content accompany by pore size and porosity increment. These results are congruous with the observation made by the group of Scaffaro et al.[39] who found that by increasing GO content in PCL scaffolds, the diameter of the scaffold's strands decreased and consequently the pore size increased.[39]

It is worthwhile to mention that the obtained values for pore size are in the range of acceptable ones (200—900 µm) for promoting osteogenesis, vascularization, and tissue ingrowth.[40] The difference between the theoretical and experimental values of pore size and porosity as well as increasing the mentioned parameters values with GO content increment could be assigned to the following reasons; i) the computational error of the device during printing processes and ii) expanding and swelling of inks during extruding from the nozzles, which is characteristic of viscoelastic polymer materials.[41,8] It has been reported that the viscosity of the composite melt could significantly be reduced by adding a tiny proportion of functionalized carbon nanoparticles.[42,43] In other word, the greater plasticity and deformation of strands in composite scaffolds may result from adding GO nanoparticles as a lubricating agent.[42] Such reduction in the viscosity of the composite melt maybe corresponded to some faults, detecting in the 3D printed composite scaffolds. Many researchers stated that this type of structural fault is inevitably occurred in extrusion-based 3D printed scaffolds.[44,45]

3.2. Characterization of 3D Printed Scaffolds

3.2.1. Physical Features of the Scaffolds

XRD analysis is conducted to assess the crystallinity of pure PCL, GO powders, as well as PCL/GO composite containing 0.25% (w/w) and 0.75% (w/w) GO (**Figure 5**a). In the XRD spectrum of GO, the absence of a peak at $2\theta = 26.43°$ corresponds to graphite and the presence of the peak at 13.28° indicates that the product is oxidized after the chemical oxidation and exfoliation, demonstrates a rise in d-spacing.[46] Pure PCL has a crystalline structure, and its characteristic peaks are observed at $2\theta = 21.08°$ and $2\theta = 24.10°$, which demonstrates that the existence of peaks corresponds to the (110) and (200) planes of the orthorhombic crystal structure of PCL.[47] Furthermore, the XRD pattern of the

PCL/GO composite films containing 0.25% and 0.75% GO also showed PCL peaks.

One of the most critical features of tissue-engineered scaffolds is their hydrophilicity, which facilitates the absorption of water and liquids and the transfer of nutrients and cellular metabolites, so the scaffolds that exhibit a high proportion of swelling are more likely to permit cell adhesion and proliferation.[48] Therefore, the wettability of tissue engineering scaffolds plays a significant role in their cell behavior.[49,50] Increasing wettability enhances initial cell adhesion, proliferation and migration.[51] Also, previous studies confirm that the hydrophilicity of the 3D printed scaffolds is subject to changes in composition.[8] Accordingly, the water contact angle measurement is a valid test to study the wettability of the 3D-printed scaffolds. As shown in Figure 5b, the contact angle of the pure PCL is found to be 114.4° ± 3.2°, which confirms the inherent hydrophobicity of the PCL. By adding 0.25% and 0.75% (w/w) GO nanoparticles, the water contact angle decreased to 85° ± 3.6° and 77° ± 3.3°, respectively. Since, oxygenated moieties cover the GO surface, it is anticipated that adding GO would improve the 3D printed PCL-based scaffolds'.[39] These results are in concurrence with the previous study, which shows that incorporating a tiny concentration of functionalized carbon nanoparticles might significantly enhance the wettability of PCL-base scaffolds.[8] Park et.al reported that adding a small amount of GO nanoparticles to PCL decreased the water contact significantly and increased hydrophilicity of PCL/GO scaffolds compared to pure PCL scaffolds.[52]

Biodegradability is one of the essential features of PCL-based porous scaffolds.[53] Generally, the speed of the tissue engineered scaffold degradation should correspond to the time and speed needed for the cell differentiation and tissue healing process.[54] PCL is a semi-crystalline bioresorbable synthetic polymer that is a member of the aliphatic polyester family, and it is known to have a prolonged degradation time of up to two years in certain conditions.[55] In order to examine the weight loss of the 3D printed scaffolds and study the influence of GO incorporation into the PCL matrix in a shorter period of time, an accelerated degradation investigation is carried out according to the method mentioned above. To this end, the 3D printed scaffolds are incubated in SBF under biological circumstances for a period of 15 days, after which their percentage of weight loss and swelling values are assessed. As shown in **Figure 6**, the scaffolds' weight loss rate after 15 days and a constant degradation rate for pure PCL and composite scaffolds containing 0.25% and 0.75% (w/w) of GO concentrations are found. Like the findings reported in wettability studies, adding GO at all concentrations enhanced
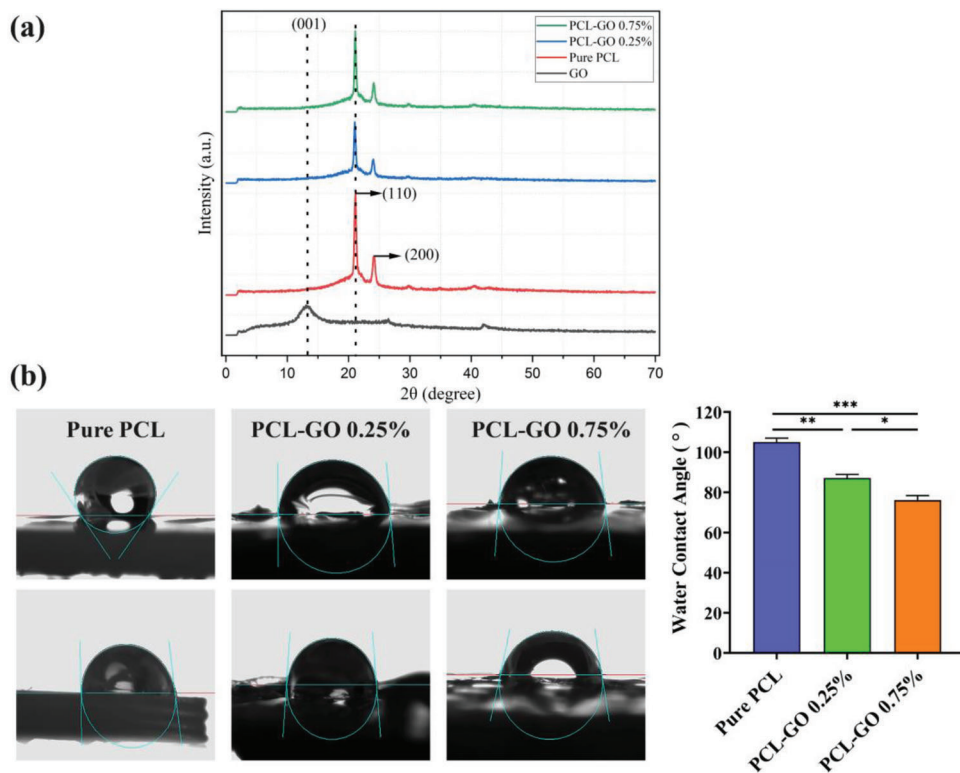
Figure 5. a) XRD pattern of GO powder, pure PCL particle and PCL/GO composite films containing 0.25% (w/w) and 0.75% (w/w) GO. b) Water contact angle test of the scaffolds.
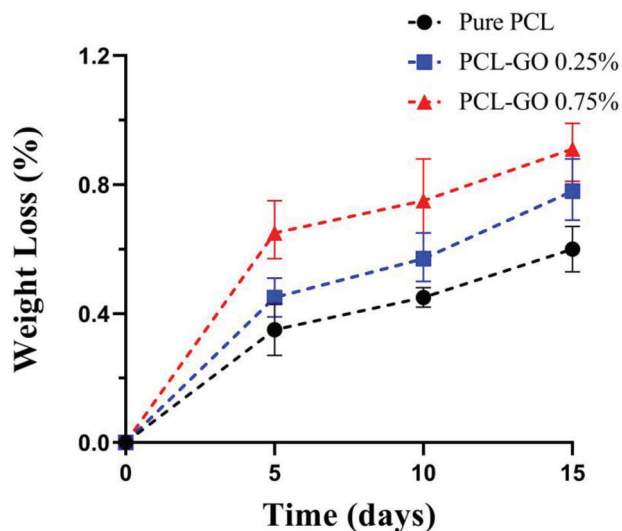
Figure 6. The degradation behavior of the 3D printed scaffolds.
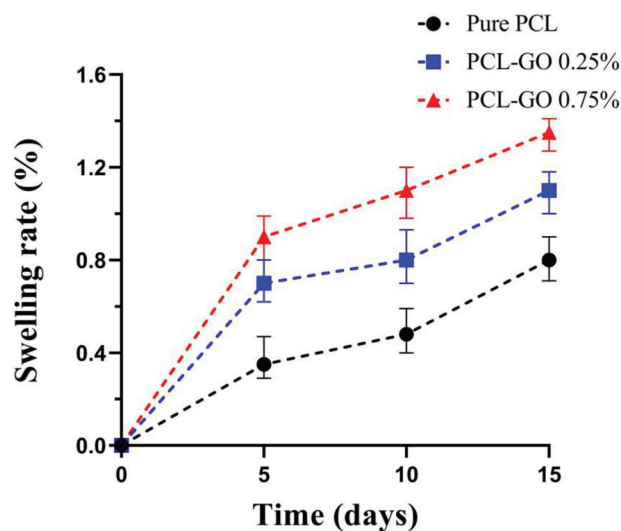
Figure 7. The swelling rate of the 3D printed scaffolds.

the weight loss percentage of the PCL/GO composite scaffolds compared to pure PCL scaffolds. The rise in weight loss percentage is in direct proportion to the GO content of the 3D printed scaffolds.[54]

The swelling rate percentage of the fabricated scaffolds also corresponded to the results of the wettability measurements and the weight loss behavior of the scaffolds. There is an increase

in the swelling rate of the PCL/GO scaffolds that is directly proportional to the GO concentrations of the scaffolds and the incubation period (**Figure 7**). It is noticeable that PCL/GO composite scaffold containing 0.75% (w/w) of GO nanoparticles shows the highest liquid uptake as a function of time. Consequently, incorporating GO into the PCL/GO composite scaffolds enhanced their wettability, hastened their degradation rate, and increased

ADVANCED
SCIENCE NEWS
www.advancedsciencenews.com

[M]acro-
[M]olecular
Materials and Engineering
Open Access
www.mame-journal.de

Table 3. Effect of mesh sizes on elastic modulus (mesh sensitivity results).

Mesh of the 5 × 5 strand design scaffold					
Mesh global size	0.6 mm	0.5 mm	0.4 mm	0.2 mm	0.15 mm
Number of tetrahedral elements	1399	1904	2865	14560	37842
Computation time	18	32	40	75	98
Elastic modulus	32.7 MPa	34.1 MPa	34.75 MPa	36.29 MPa	36.42 MPa

their fluid absorption and swelling. Thus, the ability to absorb extremely high amounts of liquids induces the transfer of more fluids to the internal structure of scaffolds and hence accelerates the hydrolytic degradation of the scaffold.[48] This is consistent with the idea that very high liquid absorption can harm the scaffold.[56]

3.3. FE Model Setup & Mesh Sensitivity Test

Compression tests are simulated via setting boundary conditions which are typical in the experimental compression test. The boundary condition and a 3D mesh are defined to convert the CAD model to the FE model. The influence of the mesh element size on the FE results is initially evaluated on the PCL scaffold with a 5 × 5 strand design under compression load. A succession of various mesh element sizes is generated depending on the same geometry; other parameters are considered similar. The scaffold's compressive elastic modulus is evaluated as an output variable to quantify the convergence when the mesh element size is lowered. **Table 3** indicates the convergency study, in which the E value, which is a macroscopic value achieved for various mesh sizes, converges to ≈36 MPa with refining the mesh sizes. The results show that the compressive elastic modulus changes by 10.5% if the smallest element size of meshing is decreased from 0.6 to 0.15 mm; The elastic modulus rarely changes by 0.4% if the mesh size is further lowered to 0.15 mm. Nevertheless, employing a mesh size of 0.1 mm needs 23 min more analysis time than using a mesh size of 0.2 mm. Consequently, it is advised to impose a minimum edge size of 0.2 mm for the tetrahedral elements to shape finite element solutions with sufficient accuracy and reasonable simulation time; So, this mesh element size is used in all of the computations.

3.4. FE Analysis

FE simulations of unrestricted ramp compression test is first conducted for 3D printed bone scaffolds. Von Mises stress and compressive Young's modulus on 3D printed PCL-based scaffolds without or with 0.25% (w/w) and 0.75% (w/w) concentration of GO nanoparticles are calculated. For linear FE analysis, the compressive Young's modulus of pure PCL and PCL/GO composite scaffolds containing 0.25% (w/w) and 0.75% (w/w) of GO nanoparticles are evaluated using the slope of the first linear area of the stress-strain plot, which is obtained from an experimental compression test. The representative compressive

Young's modulus is 39.6 ± 3.2, 32.8 ± 2.2, and 28.3 ± 2.5 MPa for pure PCL, PCL/GO 0.25%, and PCL/GO 0.75%, respectively. The elastic modulus is employed in the FE simulations with the supposition linear elastic deformation. Through the compressive Young's modulus determined from the experimental compression test, FE analysis is conducted for each model, and the mechanical behavior under compression loading is simulated. **Figure 8** demonstrates distribution of von-Mises stress as a relevant quantity for comparing the bone scaffolds with different content of GO in PCL. This confirms that the materials have a key role in the strength of the scaffolds to compressive stress. Furthermore, the value of maximum stresses is the same for scaffolds containing 5 × 5 and 4 × 4 strands, and the decrease of E value in PCL/GO composite scaffolds is observed due to the incorporation of GO into the PCL matrix.

3.5. Mechanical Characterizations of 3D Printed Scaffolds

The mechanical characteristics of tissue-engineered scaffolds depend on the inherent properties of the biomaterial, design and structure. The scaffold's mechanical characteristics have to be in accordance with the surrounding tissue's mechanical characteristics, and after implantation, the scaffold should maintain its mechanical features to rebuild hard load-bearing tissues.[57] Therefore, the uniaxial compression test is performed to find out the effect of GO incorporation and pore size on Young's modulus and compressive strength of the 3D printed scaffolds in dry and wet conditions. **Figure 9a** illustrates the stress-strain curves, Young's modulus and compressive strength of the fabricated scaffolds in dry condition. As shown in Figure 9a (step ii, step iii), Young's modulus and compressive strength of scaffolds containing 5 × 5 strands in dry condition are higher than those of 4 × 4 strands. This is in accordance with the pore size and porosity of such scaffolds. It is obvious that increasing pore size and porosity may cause reduction in mechanical properties. Therefore, the scaffold's strands number roughly impacts the Young's modulus and compressive strength values. The highest elastic modulus of 39.63 ± 2.39 MPa is achieved for pure PCL with a 5 × 5 strands design configuration in dry condition.

Increasing the GO content has an adverse effect on the compressive mechanical properties of the scaffolds in both dry and wet conditions. Unagolla et al.[16] also reported the decrement of Young's compressive modulus by the addition of 0.5% (w/w) GO to the pure PCL scaffolds. The lower compression strength of the composite scaffolds compared to pure PCL scaffolds could be related to the pore size and porosity of such scaffolds. As

**ADVANCED
SCIENCE NEWS**

www.advancedsciencenews.com

[M]acro-
olecular
Materials and **Engineering**
Open Access

www.mame-journal.de
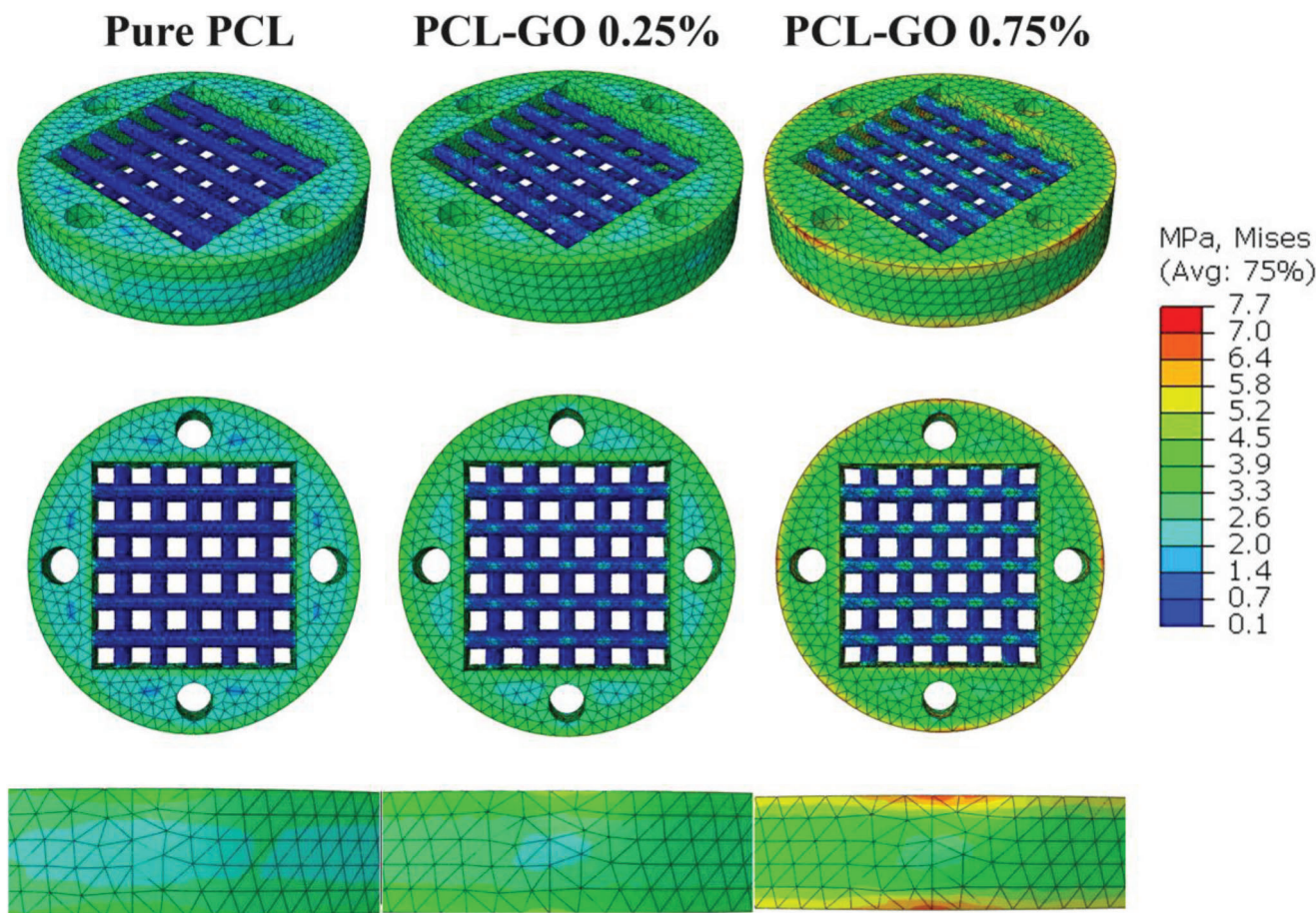
Figure 8. FE study: von-Mises stress contours evaluated for 5 × 5 strand scaffolds with 0, 0.25% (w/w) and 0.75% (w/w) concentrations of GO nanoparticle

depicted in Table 2, the pore size and porosity of composite scaffolds increased with GO increment due to decrement of strands diameter. It could be owing to unpredictable nanofibers'/strand's formation in the 3D printing process of PCL/GO composite scaffolds. Therefore, thinner fibers/strands may break sooner than thicker ones. It has been shown that when more GO is added into PCL, the space between nanosheets decreases and they are more likely to stack together via the van der Waals force.[58] Consequently, the addition of GO to the polymer solution resulted in an unstable dispersion of GO, followed by agglomeration and poor mechanical performance.[59] In the relevant study, researchers revealed that adding 0.5 and 1 wt% of GO into the PCL led to a mechanical performance decline.[6] Thus, our findings are almost in good accordance with previous studies that declared the addition of GO to the PCL can slightly reduce the mechanical properties due to the occurrence of agglomeration. The results of compressive mechanical characteristics for wet conditions in Figure 9b, indicate that the scaffolds' Young modulus and compressive strength regressed marginally compared to dry conditions for all scaffolds. Our results are in agreement with the previously reported mechanical features for PCL with graphite derivatives such PCL/GO and PCL/rGO in wet conditions.[60,61] It is worth mentioning that the length of time the scaffolds are exposed to

PBS solution is an influencing factor that should be considered. As immersion time in PBS increases, the loss in mechanical characteristics becomes more apparent.[62] Nevertheless, according to previous research, the Young modulus of bone extracellular matrix (ECM) varies from 24 kPa (osteoid matrix) to 20 GPa (compact/cortical bone).[63] Therefore, all 3D printed scaffolds studied here could be utilized as the bone matrix. Also, reported Young modulus values for natural bone varies from 20—500 MPa for cancellous/spongy, and 3000–30,000 MPa for compact/cortical bone,[64] and the current study's mechanical findings indicated that elastic modulus of all 3D printed scaffolds is in the range of cancellous/spongy bone's Young modulus values.

To validate the FE simulation, the numerical computation and experimental results are compared with each other. In Figure 9c, the FE findings related to pure PCL, and PCL/GO composite scaffolds are compared with experimental results in the linear region for specimen containing 5 × 5 strand design. In general, the linear response for both the scaffold's pure and nanocomposite material presents a good match with the examined E value. The results confirm that the numerical simulation technique is a strong tool for estimating the elastic modulus of the 3D printed scaffolds, specifically in the microstructures with single material such as pure PCL scaffolds. The compressive Young's modulus

ADVANCED
SCIENCE NEWS

www.advancedsciencenews.com

{M} acro-
olecular
Materials and Engineering
Open Access

www.mame-journal.de
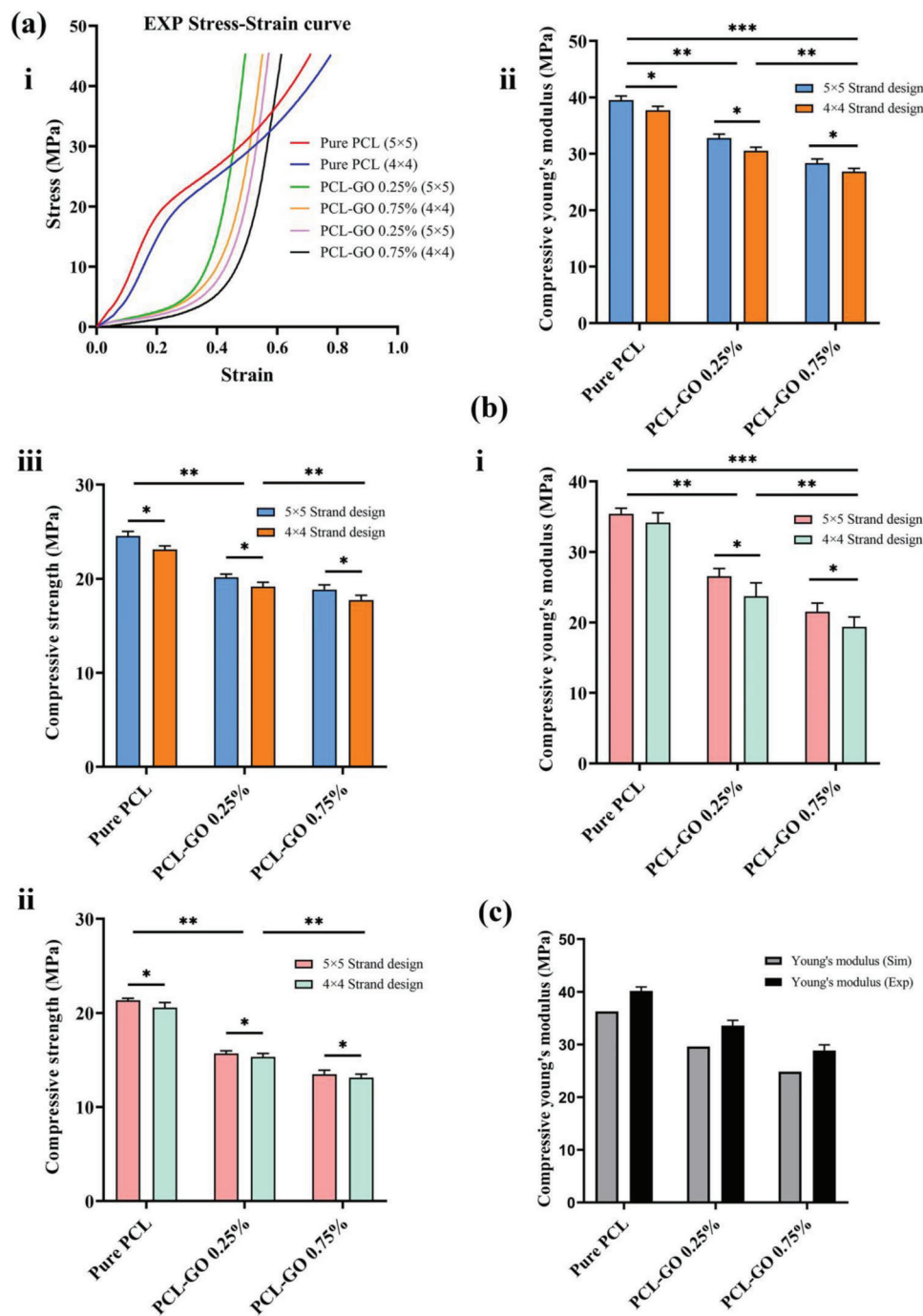
Figure 9. Mechanical investigation of the biomimetic bone scaffolds. a) Experimental study in dry condition: mechanical behavior under uniaxial compression load for scaffolds with different strand designs and GO content; i) stress-strain curve, ii) Young modulus (E), and iii) compressive strength of 3D printed scaffolds. b) Experimental study in wet condition; i) Young modulus, and ii) compressive strength. c) Validation: comparison between experimental results in dry conditions and FE simulation results.

from the linear region of FE computation for scaffolds containing 5 × 5 strands and 4 × 4 strands are in a range of 8–% relative to experimental findings. The elastic modulus of the scaffolds as computed by FE modeling is lower than that assessed experimentally, probably due to the structural irregularity of scaffolds, which is not considered in FE modeling.

3.6. In Vitro Cellular Behavior

The biocompatibility of the tissue-engineered bone scaffolds and their capability to sustain cell growth and adhesion is critical for tissue regenerative applications. In vitro experiments are related to biocompatibility and allow for the evaluation of cell toxicity.

ADVANCED SCIENCE NEWS
www.advancedsciencenews.com

acro-
olecular
Materials and Engineering
Open Access
www.mame-journal.de
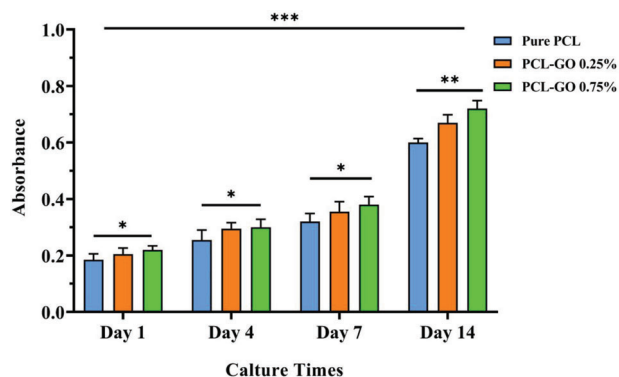
Figure 10. Absorbance values of osteoblast cells (MG-63) cultured on 3D printed bone scaffolds. Each value is the average ± standard deviation, experiments run in triplicate.

Therefore, in the current study, the cytocompatibility of the 3D printed PCL/GO composite scaffolds and the effect of GO incorporation are assessed using osteoblast cells (MG-63). The viability of osteoblast cells that are cultured on 3D printed PCL/GO composite scaffolds is determined by an MTT test. The cells viability is connected to the level of reduction, which can be evaluated with a spectrometer. **Figure 10** shows the result of the osteoblast cell viability on PCL/GO composite scaffolds after the 1st, 4th, 7th and 14th days. Our findings indicate that all 3D printed scaffolds exhibited suitable cytocompatibility with low or no cell death, and there is no significant difference in scaffolds' cell viability with different concentrations of GO (0.25% and 0.75% w/w). Results indicate that adding 0.25% and 0.75% (w/w) of GO nanoparticle in PCL/GO composite scaffolds slightly increase the cell viability compared with pure PCL scaffolds. This finding may be directly related to two functions of GO in the PCL matrix. First, it enhances the wettability of the scaffolds, and second, it accelerates osteoblasts' proliferation, adhesion, and differentiation.[65,66] Nevertheless, MTT findings revealed that cell viability did not increase remarkably as the amount of GO added increased, which is in accordance with a previous study regarding composites of PCL-based scaffolds with graphene derivatives. For instance, Faraji et al. fabricated PCL-graphene oxide (GO) scaffolds and reported that the cell viability of PCL/GO composite scaffolds does not increase significantly by adding GO to PCL polymer matrix.[67] Furthermore, some other researchers reported that doses of more than 1 wt% of graphene oxide (GO) could have a negative effect on cell viability. For example, Gohari et al. reported that PCL-reduced graphene oxide (rGO) composite scaffolds with 0.5 and 1 wt% concentration of rGO gradually increased cell viability, however when they added more amounts of rGO (1.5 wt%) in PCL matrix they observed cell viability decreased.[60] Therefore, it can be concluded that graphene oxide has dose-dependent toxicity; our results from the MTT assay showed that adding amounts less than 1% (w/w) of graphene oxide to PCL polymer matrix had no toxicity effect on PCL/GO composite scaffolds.

3.7. Cell Attachment

The cell growth, attachment, and morphology on the 3D printed PCL/GO composite scaffolds are observed by SEM on the 1st and 7th days after cultivation to confirm the biocompatibility of the samples. As shown in **Figure 11**, the SEM micrographs indicate nice cell attachment and proliferation performance in the pores of the 3D composite printed scaffolds. Osteoblast cells had widely distributed on the PCL/GO scaffolds. It is visible that the osteoblast cells had proliferated and spread on the PCL/GO composite scaffolds after 7 days. It is found that PCL-based scaffolds in the presence of GO are favorable environments for cell attachment, proliferation, and differentiation. These findings reveal that our results are in agreement with previous studies. For instance, scientists reported that incorporating 0.5% and 1% of GO into PCL nanofibers improves biocompatibility, cell attachment, and cell viability of the PCL-based scaffolds.[67] In another related study, Seyedsalehi et al. revealed that the incorporation of rGO into the PCL polymer matrix promotes the growth and proliferation of cells to a more significant extent than the PCL scaffolds.[8] Therefore, it can be concluded that PCL-based scaffolds have suitable biocompatibility properties.

4. Conclusion

In this research, a biomimetic bone scaffold with cortical and cancellous regions along with Haversian channels was designed, and 3D printed. Furthermore, the effects of incorporation of 0.25% (w/w) and 0.75% (w/w) GO concentration on morphological properties, geometry, structure, crystallinity, wettability, biodegradability, mechanical characteristics both in the dry and wet conditions, biocompatibility, and cell attachment of the scaffolds were investigated by experiments. The SEM images showed that scaffolds have well-defined architecture and interconnected pore networks. Moreover, the pore size and porosity of the scaffolds increased with increasing GO and decreasing the number of strands in the middle section of the scaffolds. Additionally, SEM images indicated a decrease in complex viscosity of PCL/GO composite ink containing 0.25% and 0.75% GO concentrations that caused a decrease in the average diameter of strands if compared with higher pure PCL ink; consequently, the average pore size of PCL/GO composite scaffolds increased. The presence of GO nanoparticles changed the surface properties of the 3D printed scaffolds from hydrophobic to hydrophilic. According to the contact angles measurements, GO nanoparticles' considerable hydrophilic features enhanced the wettability of PCL/GO composite scaffolds compared to pure PCL scaffolds. Adding 0.5% and 0.75% (w/w) of GO into the PCL polymer matrix increases the swelling ratio and degradation time of the 3D printed scaffolds. The mechanical compression test results showed that Young's modulus and compressive strength of PCL/GO composite scaffolds decreased with GO content increment both for dry and wet conditions. The FE simulation data indicated that the simulation values were in good correlation with experimental results. The high cell viability and attachment of MG-63 osteoblast cells revealed that PCL/GO composite scaffolds have such acceptable biocompatibility that they can be considered a promising candidate for bone tissue engineering applications. This research provides valuable data about the printability, microstructure features, wettability, mechanical characteristics, and biological properties of 3D printed PCL/GO scaffolds with the biomimetic design. This study would be expected to pave the way for the design of more efficient scaffolds for bone tissue engineering.

**ADVANCED
SCIENCE NEWS**

www.advancedsciencenews.com

{M} acro-
molecular
Materials and Engineering
Open Access

www.mame-journal.de

PCL-GO 0.25%   PCL-GO 0.75%
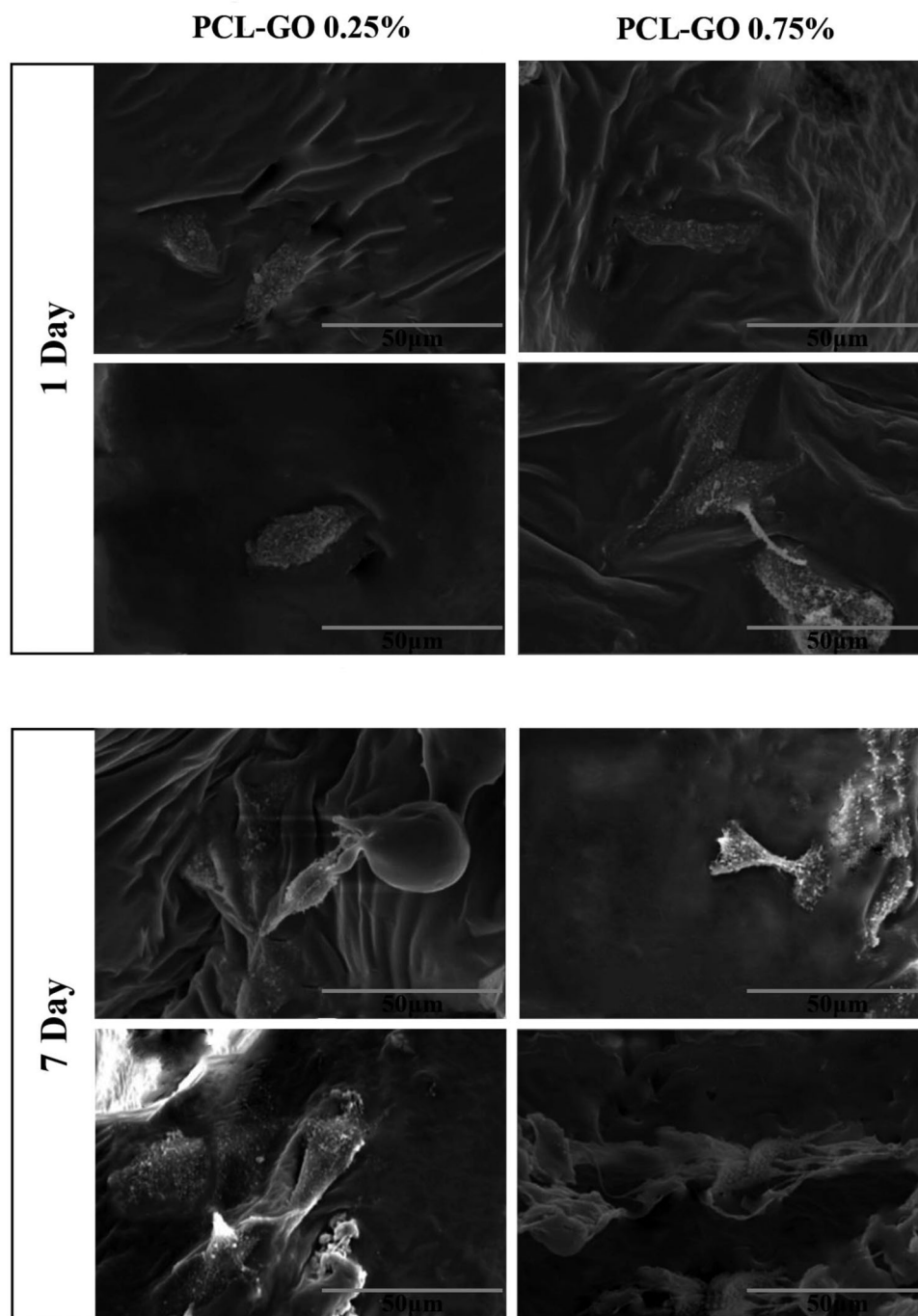
Figure 11. SEM images of osteoblast cell attachment and their morphology on PCL/GO composite scaffolds.

Conflict of Interest

The authors declare no conflict of interest.

Data Availability Statement

All data are included in the paper.

Keywords

[1] W. Wang, K. W. Yeung, *Bioact. Mater.* **2017**, *2*, 224.

[2] R. Noroozi, M. A. Shamekhi, R. Mahmoudi, A. Zolfagharian, F. Asgari, A. Mousavizadeh, M. Bodaghi, A. Hadi, N. Haghighipour, *Biomed. Mater.* **2022**, *17*, 045024.

[3] S. Bahrami, A. Solouk, D. Duprez, H. Mirzadeh, *Macromol. Mater. Eng.* **2022**, *307*, 2100584.

[4] P. R. L. Nalesso, W. Wang, Y. Hou, L. Bagne, A. T. Pereira, J. V. Helaehil, T. A. M. de Andrade, G. B. Chiarotto, P. Bártolo, G. F. Caetano, *Bioprinting* **2021**, *24*, e00164.

[5] I. K. Sabree: *Fabrication of Bioactive Glass Scaffolds by Stereolithography for Bone Tissue Engineering*, The University of Manchester, Manchester UK **2014**.

[6] J. Song, H. Gao, G. Zhu, X. Cao, X. Shi, Y. Wang, *Carbon* **2015**, *95*, 1039.

[7] M. Mozafari, M. Gholipourmalekabadi, N. Chauhan, N. Jalali, S. Asgari, J. Caicedoa, A. Hamlekhan, A. Urbanska, *Mater. Sci. Eng., C* **2015**, *50*, 117.

[8] A. Seyedsalehi, L. Daneshmandi, M. Barajaa, J. Riordan, C. T. Laurencin, *Sci. Rep.* **2020**, *10*, 1.

[9] G. M. Cunniffe, P. J. Díaz-Payno, E. J. Sheehy, S. E. Critchley, H. V. Almeida, P. Pitacco, S. F. Carroll, O. R. Mahon, A. Dunne, T. J. Levingstone, *Biomaterials* **2019**, *188*, 63.

[10] J. Li, M. Chen, X. Wei, Y. Hao, J. Wang, *Materials* **2017**, *10*, 831.

[11] B. Stolz, M. Mader, L. Volk, T. Steinberg, R. Mülhaupt, *Macromol. Mater. Eng.* **2021**, *306*, 2000541.

[12] D. Liu, W. Nie, D. Li, W. Wang, L. Zheng, J. Zhang, J. Zhang, C. Peng, X. Mo, C. He, *Chem. Eng. J.* **2019**, *362*, 269.

[13] B. Felice, M. A. Sánchez, M. C. Socci, L. D. Sappia, M. I. Gómez, M. K. Cruz, C. J. Felice, M. Martí, M. I. Pividori, G. Simonelli, *Mater. Sci. Eng., C* **2018**, *93*, 724.

[14] N. Akhigan, N. Najmoddin, H. Azizi, M. Mohammadi, *Int. J. Polym. Mater. Polym. Biomater.* **2022**, https://doi.org/10.1080/00914037.2022.2100373.

[15] S. Kohzadi, N. Najmoddin, H. Baharifar, M. Shabani, *Diamond Relat. Mater.* **2022**, *127*, 109149.

[16] J. M. Unagolla, A. C. Jayasuriya, *Mater. Sci. Eng., C* **2019**, *102*, 1.

[17] J. Zhang, H. Eyisoylu, X.-H. Qin, M. Rubert, R. Müller, *Acta Biomater.* **2021**, *121*, 637.

[18] S. Kashte, R. Sharma, S. Kadam, *J. Bioact. Compat. Polym.* **2020**, *35*, 57.

[19] F. Rostami, E. Tamjid, M. Behmanesh, *Mater. Sci. Eng., C* **2020**, *115*, 111102.

[20] W. Wang, J. R. P. Junior, P. R. L. Nalesso, D. Musson, J. Cornish, F. Mendonça, G. F. Caetano, P. Bártolo, *Mater. Sci. Eng., C* **2019**, *100*, 759.

[21] A. P. Castro, J. Santos, T. Pires, P. R. Fernandes, *Macromol. Mater. Eng.* **2020**, *305*, 2000487.

[22] Y. Zamani, G. Amoabediny, J. Mohammadi, H. Seddiqi, M. N. Helder, B. Zandieh-Doulabi, J. Klein-Nulend, J. H. Koolstra, *J. Mech. Behav. Biomed. Mater.* **2020**, *104*, 103638.

[23] A. Di Luca, A. Longoni, G. Criscenti, C. Mota, C. van Blitterswijk, L. Moroni, *Biofabrication* **2016**, *8*, 045007.

[24] X. Li, Y.-Z. Xiong, H. Zhang, R.-N. Gao, *Mater. Lett.* **2021**, *282*, 128670.

[25] M. Zhang, R. Lin, X. Wang, J. Xue, C. Deng, C. Feng, H. Zhuang, J. Ma, C. Qin, L. Wan, *Sci. Adv.* **2020**, *6*, eaaz6725.

[26] I. Sahafnejad-Mohammadi, M. Karamimoghadam, A. Zolfagharian, M. Akrami, M. Bodaghi, *J. Braz. Soc. Mech. Sci. Eng.* **2022**, *44*, 1.

[27] A. Zimmerling, Z. Yazdanpanah, D. M. Cooper, J. D. Johnston, X. Chen, *Biomater. Res.* **2021**, *25*, 1.

[28] M. Bodaghi, A. Damanpack, W. Liao, *Mater. Des.* **2017**, *135*, 26.

[29] J. K. Placone, A. J. Engler, *Adv. Healthcare Mater.* **2018**, *7*, 1701161.

[30] B. Ostrowska, A. Di Luca, L. Moroni, W. Swieszkowski, *J. Biomed. Mater. Res., Part A* **2016**, *104*, 991.

[31] L. Baldino, F. Naddeo, S. Cardea, A. Naddeo, E. Reverchon, *J. Mech. Behav. Biomed. Mater.* **2015**, *51*, 225.

[32] S. Barui, S. Chatterjee, S. Mandal, A. Kumar, B. Basu, *Mater. Sci. Eng., C* **2017**, *70*, 812.

[33] J. Wieding, A. Wolf, R. Bader, *J. Mech. Behav. Biomed. Mater.* **2014**, *37*, 56.

[34] https://imagej.nih.gov/ij/.

[35] P. Feng, P. Wu, C. Gao, Y. Yang, W. Guo, W. Yang, C. Shuai, *Adv. Sci.* **2018**, *5*, 1700817.

[36] L. Zhang, G. Yang, B. N. Johnson, X. Jia, *Acta Biomater.* **2019**, *84*, 16.

[37] H. Seddiqi, A. Saatchi, G. Amoabediny, M. N. Helder, S. A. Ravasjani, M. S. H. Aghaei, J. Jin, B. Zandieh-Doulabi, J. Klein-Nulend, *Comput. Biol. Med.* **2020**, *124*, 103826.

[38] Z. Bashiri, M. Gholipourmalekabadi, R. Falak, I. Amiri, H. Asgari, N. P. S. Chauhan, M. Koruji, *Int. J. Biol. Macromol.* **2022**, *217*, 824.

[39] R. Scaffaro, F. Lopresti, A. Maio, L. Botta, S. Rigoglioso, G. Ghersi, *Composites, Part A* **2017**, *92*, 97.

[40] A. J. Salgado, O. P. Coutinho, R. L. Reis, *Macromol. Biosci.* **2004**, *4*, 743.

[41] H. Yuk, X. Zhao, *Adv. Mater.* **2018**, *30*, 1704028.

[42] D. Dias, A. C. Vale, E. P. Cunha, M. C. Paiva, R. L. Reis, C. Vaquette, N. M. Alves, *J. Biomed. Mater. Res., Part B* **2021**, *109*, 961.

[43] J. A. Martins, V. S. Cruz, M. C. Paiva, *Macromolecules* **2011**, *44*, 9804.

[44] S. Wickramasinghe, T. Do, P. Tran, *Polymers* **2020**, *12*, 1529.

[45] C. Oztan, R. Karkkainen, M. Fittipaldi, G. Nygren, L. Roberson, M. Lane, E. Celik, *J. Compos. Mater.* **2019**, *53*, 271.

[46] G. Surekha, K. V. Krishnaiah, N. Ravi, R. P. Suvarna, *J. Phys.: Conf. Ser.* **2020**, *1*, 012012.

[47] S. U. Maheshwari, V. K. Samuel, N. Nagiah, *Ceram. Int.* **2014**, *40*, 8469.

[48] Z. Bashiri, I. Amiri, M. Gholipourmalekabadi, R. Falak, H. Asgari, C. B. Maki, A. Moghaddaszadeh, M. Koruji, *Biomater. Sci.* **2021**, *9*, 3465.

[49] M. Lin, H. Wang, C. Ruan, J. Xing, J. Wang, Y. Li, Y. Wang, Y. Luo, *Biomacromolecules* **2015**, *16*, 973.

[50] C. Pinese, S. Jebors, P. E. Stoebner, V. Humblot, P. Verdié, L. Causse, X. Garric, H. Taillades, J. Martinez, A. Mehdi, *Mater. Today Chem.* **2017**, *4*, 73

[51] A. S. K. Kiran, T. S. Kumar, R. Sanghavi, M. Doble, S. Ramakrishna, *Nanomaterials* **2018**, *8*, 860.

[52] J. Park, S. Park, J. E. Kim, K.-J. Jang, H. Seonwoo, J. H. Chung, *Polymers* **2021**, *13*, 797.

[53] A. Yazdanpanah, Z. Madjd, M. Pezeshki-Modaress, Z. Khosrowpour, P. Farshi, L. Eini, J. Kiani, M. Seifi, S. C. Kundu, R. Ghods, *Artif. Organs* **2022**, *46*, 1040.

[54] A. Aidun, A. Safaei Firoozabady, M. Moharrami, A. Ahmadi, N. Haghighipour, S. Bonakdar, S. Faghihi, *Artif. Organs* **2019**, *43*, E264.

[55] C. X. Lam, M. M. Savalani, S.-H. Teoh, D. W. Hutmacher, *Biomed. Mater.* **2008**, *3*, 034108.

[56] V. Guarino, T. Caputo, R. Altobelli, L. Ambrosio, *AIMS Mater. Sci.* **2015**, *2*, 497.

[57] S. Prasadh, R. C. W. Wong, *Oral Sci. Int.* **2018**, *15*, 48.

[58] S. Ramazani, M. Karimi, *Mater. Sci. Eng., C* **2015**, *56*, 325.

[59] G.-s. Wang, Z.-y. Wei, L. Sang, G.-y. Chen, W.-x. Zhang, X.-f. Dong, M. Qi, *Chin. J. Polym. Sci.* **2013**, *31*, 1148.

[60] P. H. M. Gohari, M. H. Nazarpak, M. Solati-Hashjin, *Mater. Today Commun.* **2021**, *27*, 102287.

[61] F. Lopresti, A. Maio, L. Botta, R. Scaffaro. in: AIP Conference Proceedings **2016**, vol. *1*, p. 020105. AIP Publishing LLC, Melville USA.

[62] S. Sánchez-González, N. Diban, A. Urtiaga, *Membranes* **2018**, *8*, 12.

[63] A. Padhi, A. S. Nain, *Ann. Biomed. Eng.* **2020**, *48*, 1071.

[64] R. Mahdavi, G. Belgheisi, M. Haghbin-Nazarpak, M. Omidi, A. Khojasteh, M. Solati-Hashjin, *J. Mater. Sci.: Mater. Med.* **2020**, *31*, 1.

[65] I. F. Wahab, S. I. A. Razak, N. S. Azmi, F. N. Dahli, A. H. M. Yusof, N. M. Nayan, *Advances in Carbon Nanostructures*, IntechOpen, London, United Kingdom **2016**, https://doi.org/10.5772/64055.

[66] A. O. Basar, V. Sadhu, H. T. Sasmazel, *Biomed. Mater.* **2019**, *14*, 045012.

[67] S. Faraji, N. Nowroozi, A. Nouralishahi, J. S. Shayeh, *Life Sci.* **2020**, *257*, 118062.